Article

Design of Cationic Conjugated Polyelectrolytes for DNA Concentration Determination

Chunyan Chi, Alexander Mikhailovsky, and Guillermo C. Bazan

J. Am. Chem. Soc., **2007**, 129 (36), 11134-11145• DOI: 10.1021/ja072471s • Publication Date (Web): 18 August 2007

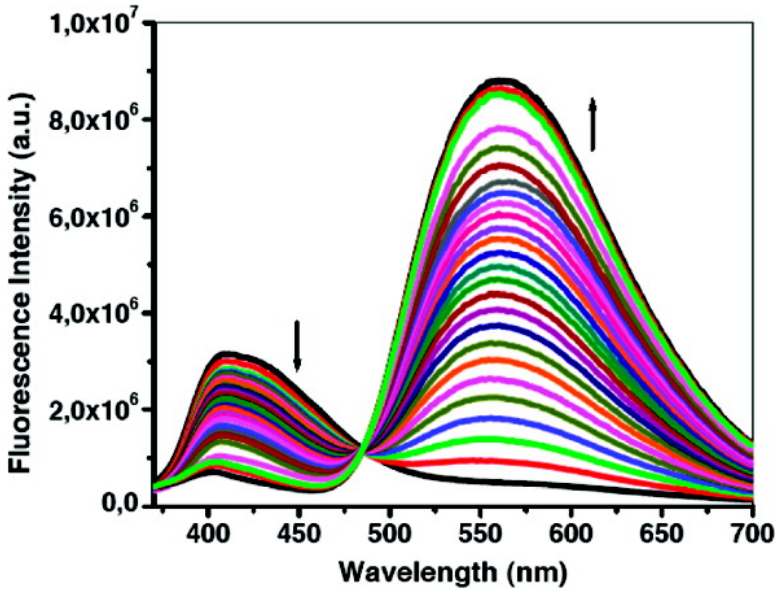

More About This Article

Additional resources and features associated with this article are available within the HTML version:

- Supporting Information
- Links to the 12 articles that cite this article, as of the time of this article download
- Access to high resolution figures
- Links to articles and content related to this article
- Copyright permission to reproduce figures and/or text from this article

View the Full Text HTML

J|A|C|S
ARTICLES
Published on Web 08/18/2007

Design of Cationic Conjugated Polyelectrolytes for DNA Concentration Determination

Chunyan Chi, Alexander Mikhailovsky, and Guillermo C. Bazan*

Contribution from the Departments of Chemistry and Biochemistry and Materials, Institute for Polymers and Organic Solids, University of California, Santa Barbara, California 93106

Received April 9, 2007; E-mail: bazan@chem.ucsb.edu

Abstract: Cationic conjugated polyelectrolytes **poly1$_{10}$** and **poly1$_{20}$** were designed, synthesized, and characterized with the anticipation of function in the determination of double-stranded DNA concentration [dsDNA]. Their structures contain a π-delocalized optically active backbone composed of phenylene−fluorene segments copolymerized with 2,1,3-benzothiadiazole (BT) units and charged pendant groups that allow excellent solubility in water. The subscript in **poly1$_x$** refers to the molar percent of BT units in the chain. Addition of dsDNA to **poly1$_{10}$** or **poly1$_{20}$** results in a change in the color of emission from blue to green. These spectral changes can be treated to obtain the parameter δ, which can be used to generate calibration curves that indicate [dsDNA]. Analysis of photoluminescence spectra reveals that dsDNA addition gives rise to more efficient FRET from blue emitting segments to the BT sites, an increase in the BT emission quantum yield, and partial quenching of the phenylene−fluorene segments. Studies were also carried out to maximize the range of [dsDNA] determination. We find that by combining the response from two different initial concentrations of **poly1$_{10}$**, it is possible to generate calibration curves that respond with a difference in [dsDNA] of over 7 orders of magnitude.

Introduction

Conjugated polyelectrolytes (CPEs) are polymers containing a π-conjugated backbone and functional groups that ionize in high dielectric media.[1] These materials combine the semiconducting and photon harvesting properties of electronically delocalized polymers with the charge-mediated behavior of polyelectrolytes. CPEs offer interesting possibilities for optoelectronic applications, including the formation of surface dipoles,[2] ion motion to compensate injected charges,[3] and solubility in polar solvents to fabricate multilayer structures by alternating solvent polarity with minimum disturbance of underlying layers.[4] Furthermore, recent studies have shown that the charge carrier mobilities in CPEs are similar or larger than those in neutral conjugated polymers of similar structure.[5]

Substantial efforts have been placed in developing homogeneous and heterogeneous biosensor assays that take advantage of the optical amplification afforded by CPEs.[6] The ionic groups are essential for increasing water solubility, an important requirement for biological detection.[7,8] It has been possible through substantially different strategies to design assays that are specific to proteins,[9,10] DNA,[11] and RNA.[12] One particular sensing strategy takes advantage of the large optical cross section of CPEs in combination with a biomolecular recognition event that triggers fluorescence resonance energy transfer (FRET)[13] to a reporting, or "signaling", dye. Electrostatic interactions are

(1) (a) Pinto, M. R.; Schanze, K. S. *Synthesis* **2002**, *9*, 1293.
(2) (a) Wu, H. B.; Huang, F.; Mo, Y. Q.; Yang, W.; Wang, D. L.; Peng, J. B.; Cao, Y. *Adv. Mater.* **2004**, *16*, 1826. (b) Ma, W. L.; Iyer, P. K.; Gong, X.; Liu, B.; Moses, D.; Bazan, G. C.; Heeger, A. J. *Adv. Mater.* **2005**, *17*, 274. (c) Yang, R.; Wu, H.; Cao, Y.; Bazan, G. C. *J. Am. Chem. Soc.* **2006**, *128*, 14422.
(3) Edman, L.; Pauchard, M.; Liu, B.; Bazan, G. C.; Moses, D.; Heeger, A. J. *Appl. Phys. Lett.* **2003**, *82*, 3961.
(4) (a) Gong, X.; Wang, S.; Moses, D.; Bazan, G. C.; Heeger, A. J. *Adv. Mater.* **2005**, *17*, 2053. (b) Kim, S.; Jackiw, J.; Robinson, E.; Schanze, K. S.; Reynolds, J. R.; Baur, J.; Rubner, M. F.; Boils, D. *Macromolecules* **1998**, *31*, 964. (c) Ferreira, M.; Rubner, M. F. *Macromolecules* **1995**, *28*, 7107. (d) Cimrova, V.; Schmidt, W.; Rulkens, R.; Schulze, M.; Meyer, W.; Neher, D. *Adv. Mater.* **1996**, *8*, 585. (e) Baur, J. W.; Kim, S.; Balanda, P. B.; Reynolds, J. R.; Rubner, M. F. *Adv. Mater.* **1998**, *10*, 1452. (f) Huang, F.; Wu, H.; Wang, D.; Yang, W.; Cao, Y. *Chem. Mater.* **2004**, *16*, 708. (g) Huang, F.; Hou, L.; Wu, H.; Wang, X.; Shen, H.; Cao, W.; Yang, W.; Cao, Y. *J. Am. Chem. Soc.* **2004**, *126*, 9845. (h) Chang, S. C.; Bharathan, J.; Yang, Y.; Helgeson, R.; Wudl, F.; Ramey, M. B.; Reynold, J. R. *Appl. Phys. Lett.* **1998**, *73*, 2561. (i) Ho, P. K. H.; Kim, J. S.; Burroughes, J. H.; Becker, H.; Li, S. F. Y.; Brown, T. M.; Cacialli, F.; Friend, R. H. *Nature* **2000**, *404*, 481.
(5) Yang, R.; Garcia, A.; Korystov, D.; Mikhailovsky, A.; Bazan, G. C.; Nguyen, T. Q. *J. Am. Chem. Soc.* **2006**, *128*, 16532.
(6) (a) McUuade, D. T.; Pullen, A. E.; Swager, T. M. *Chem. Rev.* **2000**, *100*, 2537. (b) Liu, B.; Bazan, G. C. *Chem. Mater.* **2004**, *16*, 4467. (c) Zheng, J.; Swager, T. M. *Adv. Polym. Sci.* **2005**, *177*, 151. (d) Faïd, K.; Leclerc, M. *Chem. Commun.* **1996**, 2761 (e) Doré, K.; Dubus, S.; Ho, H. A.; Lévesque, I.; Brunette, M.; Corbeil, G.; Boissinot, M.; Boivin, G.; Bergeron, M. G.; Boudreau, D.; Leclerc, M. *J. Am. Chem. Soc.* **2004**, *126*, 4240. (f) Nilsson, K. P. R.; Inganäs, O. *Macromolecules* **2004**, *37*, 9109. (g) Nilsson, K. P. R.; Rydberg, J.; Baltzer, L.; Inganäs, O. *Proc. Natl. Acad. Sci. U.S.A.* **2003**, *100*, 10170. (h) Chen, L.; McBranch, D. W.; Wang, H.-L.; Helgeson, R.; Wudl, F.; Whitten, D. G. *Proc. Natl. Acad. Sci. U.S.A.* **1999**, *96*, 12287. (i) Wang, S.; Gaylord, B. S.; Bazan, G. C. *J. Am. Chem. Soc.* **2004**, *126*, 5446. (j) Achyuthan, K. E.; Bergstedt, T. S.; Chen, L.; Jones, R. M.; Kumaraswamy, S.; Kushon, S. A.; Ley, K. D.; Lu, L.; McBranch, D.; Mukundan, H.; Rininsland, F.; Shi, X.; Xia, W.; Whitten, D. G. *J. Mater. Chem.* **2005**, *15*, 2648.
(7) (a) Kim, I. B.; Dunkhorst, A.; Gilbert, J.; Bunz, U. H. F.; *Macromolecules* **2005**, *38*, 4560. (b) Le Floch, F.; Ho, H. A.; Harding-Lepage, P.; Bedard, M.; Neagu-Plesu, R.; Leclerc, M. *Adv. Mater.* **2005**, *17*, 1251. (c) Ho, H. A.; Bers-Aberem, M.; Leclerc, M. *Chem.—Eur. J.* **2005**, *11*, 1718. (d) Nilsson, K. P. R.; Inganäs, O. *Nat. Mater.* **2003**, *2*, 419. (e) Herland, A.; Nilsson, K. P. R.; Olsson, J. D. M.; Hammarstrom, P.; Konradsson, P.; Inganäs, O. *J. Am. Chem. Soc.* **2005**, *127*, 2317.
(8) (a) Xu, Q.; Wang, S.; Korystov, D.; Mikhailovsky, A.; Bazan, G. C.; Moses, D.; Heeger, A. J. *Proc. Natl. Acad. Sci. U.S.A.* **2005**, *102*, 530. (b) Tang, Y.; Feng, F.; He, F.; Wang, S.; Li, Y.; Zhu, D. *J. Am. Chem. Soc.* **2006**, *128*, 14972.

10.1021/ja072471s CCC: $37.00

Chart 1. Molecular Structure of **PFPB$_x$**

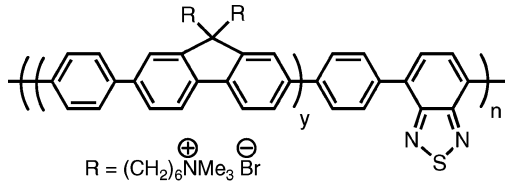

PFPB$_x$, x = 100/(y + 1)

essential for controlling the average distance between optical partners and thereby the sensitivity and selectivity of the assay. The overall process is complex, and there are substantial gaps in our understanding, in particular the general shape, size, and molecular organization on the resulting aggregates. Despite the supramolecular complexity, molecular design has produced a variety of structures for optimizing assays, which allow one to control the color of emission,[14] the ability of the main chain to adapt to the secondary structure of biomolecules,[15] the chain dependence of the recognition event,[16] and the ratio of FRET vs photoinduced charge transfer.[17]

Structure−function relationship studies have shown that poly-((9,9-bis(6′-*N*,*N*,*N*-trimethylammoniumbromide)hexyl)fluorene-*co*-*alt*-1,4,-phenylene) (**PFPB$_x$** in Chart 1) containing a fractional substitution of fluorene monomers with 2,1,3-benzothiadiazole (BT), in combination with dye-labeled PNA probes, can be used in multicolor assays. The subscript "*x*" refers to the percentage of phenylene−BT units in the main chain, while 100 − *x* % corresponds to the fraction due to phenylene−fluorene segments. One important feature of **PFPB$_x$** is that its emission is concentration dependent; blue emission occurs under dilute conditions while green emission is observed in more concentrated solutions. The working hypothesis is that FRET from the blue-emitting phenylene−fluorene segments to the green-emitting BT sites occurs more efficiently via *inter*chain contacts in aggregates than that via the *intra*chain process within more isolated polymer chains.[18]

Addition of negatively charge polyelectrolytes to **PFPB$_x$** induces complexation as a result of cooperative electrostatic interactions.[19] As illustrated in Figure 1, the local concentration of **PFPB$_x$** in these aggregates is increased, thereby shifting the emission from blue to green. Such optical changes can be induced with dsDNA or single-stranded DNA (ssDNA), and the spectral features can be analyzed to determine the concentration of DNA in an unknown sample.[20] The overall process provides an alternative method to emissive intercalating dyes for measuring [DNA] under conditions too dilute for absorbance spectroscopy ($\geq 3.8 \times 10^{-7}$ M in base pairs, bps, or 250 ng/mL).[21,22] Such information is important in a variety of applications ranging from the quantification of polymerase chain reaction products to the evaluation of biosensors.[23]

Using **PFPB$_7$** one obtains an upper detection limit for [dsDNA] of 1.5×10^{-7} M base pairs (bps) and a lower detection limit of 6.0×10^{-10} M bps. For comparison, commercially available fluorescence methods using intercalating dyes can detect concentrations as low as 3.8×10^{-11} M bps (25 pg/mL) for dsDNA and 3.0×10^{-10} M in bases (100 pg/mL) for ssDNA.[24−31] The upper limit for **PFPB$_7$** is restricted by the stoichiometric relationship between negative and positive charges. Increasing [**PFPB$_7$**] provides the appearance of the green emission in the absence of dsDNA, and the assay becomes less reliable. Factors that determine the lower detection limit remain poorly understood at this time.

In this contribution we disclose the design of cationic conjugated polyelectrolytes with optimized molecular features that allow for the determination of [dsDNA] from 3×10^{-12} to 2×10^{-5} M. We start by providing a rationale for the choice of structure and an analysis of the intrinsic optical properties of these new materials as a function of experimental conditions. We then examine perturbations in emission properties upon complexation with dsDNA and show that the polyelectrolyte complexation leads to changes in FRET efficiencies, optical

(9) (a) Dwight, S. J.; Gaylord, B. S.; Hong, J. W.; Bazan, G. C. *J. Am. Chem. Soc.* **2004**, *126*, 16850. (b) An, L.; Tang, Y.; Wang, S.; Li, Y.; Zhu, D. *Macromol. Rapid Commun.* **2006**, *27*, 993. (c) Wang, D.; Gong, X.; Heeger, P. S.; Rininsland, F.; Bazan, G. C.; Heeger, A. J. *Proc. Natl. Acad. Sci. U.S.A.* **2002**, *99*, 49. (d) Abérem, M. B.; Najari, A.; Ho, H. A.; Gravel, J. F.; Nobert, P.; Boudreau, D.; Leclerc, M. *Adv. Mater.* **2006**, *18*, 2703. (e) Ho, H. A.; Leclerc, M. *J. Am. Chem. Soc.* **2004**, *126*, 1384. (f) Floch, F. L.; Ho, H. A.; Leclerc, M. *Anal. Chem.* **2006**, *78*, 4727.

(10) (a) Nilsson, K. P. R.; Herland, A.; Hammarström, P.; Inganäs, O. *Biochemistry* **2005**, *44*, 3718. (b) Nilsson, K. P. R.; Hammarström, P.; Ahlgren, F.; Herland, A.; Schnell, E. A.; Lindgren, M.; Westermark, G. T.; Inganäs, O. *ChemBioChem* **2006**, *7*, 1096. (c) Pinto, M. R.; Schanze, K. S. *Proc. Natl. Acad. Sci. U.S.A.* **2004**, *101*, 7505. (d) Kim, I. B.; Dunkhorst, A.; Bunz, U. H. F. *Langmuir* **2005**, *21*, 7985.

(11) (a) Ho, H. A.; Boissinot, M.; Bergeron, M. G.; Corbeil, G.; Dore, K.; Boudreau, D.; Leclerc, M. *Angew. Chem., Int. Ed.* **2002**, *41*, 1548. (b) Gaylord, B. S.; Heeger, A. J.; Bazan, G. C. *Proc. Natl. Acad. Sci. U.S.A.* **2002**, *99*, 10954. (c) Gaylord, B. S.; Massie, M. R.; Feinstein, S. C.; Bazan, G. C. *Proc. Natl. Acad. Sci. U.S.A.* **2005**, *102*, 34. (d) Ho, H. A.; Doré, K.; Boissinot, M.; Bergeron, M. G.; Tanguay, R. M.; Boudreau, D.; Leclerc, M. *J. Am. Chem. Soc.* **2005**, *127*, 12673. (e) Baker, E. S.; Hong, J. W.; Gaylord, B. S.; Bazan, G. C.; Bowers, M. T. *J. Am. Chem. Soc.* **2006**, *128*, 8484. (f) Xu, Q.-H.; Gaylord, B. S.; Wang, S.; Bazan, G. C.; Moses, D.; Heeger, A. J. *Proc. Natl. Acad. Sci. U.S.A.* **2004**, *101*, 11634. (g) Gaylord, B. S.; Heeger, A. J.; Bazan, G. C. *J. Am. Chem. Soc.* **2003**, *125*, 896. (h) He, F.; Tang, Y.; Wang, S.; Li, Y.; Zhu, D. *J. Am. Chem. Soc.* **2005**, *127*, 12343. (i) He, F.; Tang, Y.; Yu, M.; Feng, F.; An, L.; Sun, H.; Wang, S.; Li, Y.; Zhu, D.; Bazan, G. C. *J. Am. Chem. Soc.* **2006**, *128*, 6764.

(12) (a) Liu, B.; Baudrey, S.; Jaeger, L.; Bazan, G. C. *J. Am. Chem. Soc.* **2004**, *126*, 4076. (b) Wang, S.; Bazan, G. C. *Adv. Mater.* **2003**, *15*, 1425.

(13) (a) Förster, T. *Discuss. Faraday Soc.* **1959**, *27*, 7. (b) Lakowicz, J. R. *Principles of Fluorescence Spectroscopy*, 2nd ed.; Kluwer Academic/Plenum Publications: New York, 1999. (c) Valeur, B. *Molecular Fluorescence*; Wiley-VCH: Weinheim, 2002.

(14) Liu, B.; Bazan, G. C. *J. Am. Chem. Soc.* **2004**, *126*, 1942.

(15) Liu, B.; Wang, S.; Bazan, G. C.; Mikhailovsky, A. *J. Am. Chem. Soc.* **2003**, *125*, 13306.

(16) Wang, S.; Liu, B.; Gaylord, B. S.; Bazan, G. C. *Adv. Funct. Mater.* **2003**, *13*, 463.

(17) Liu, B.; Bazan, G. *J. Am. Chem. Soc.* **2006**, *128*, 1188.

(18) (a) Beljonne, D.; Pourtois, G.; Silva, C.; Hennebicq, E.; Herz, L. M.; Friend, R. H.; Scholes, G. D.; Setayesh, S.; Müllen, K.; Brédas, J. L. *Proc. Natl. Acad. Sci. U.S.A.* **2002**, *99*, 10982. (b) Schwartz, B. J.; Nguyen, T.-Q.; Wu, J.; Tolbert, S. H. *Synth. Met.* **2001**, *116*, 35.

(19) (a) *Self-Assembling Complexes for Gene Delivery, From Laboratory to Clinical Trial*; Kabanov, A. V., Felgner, P. L., Seymour, L. W., Eds.; John Wiley: Chichester, 1998. (b) Gössl, I.; Shu, L.; Shülter, A. D.; Rabe, J. P. *J. Am. Chem. Soc.* **2002**, *124*, 6860. (c) Wang, Y.; Dubin, P. L.; Zhang, H. *Langmuir* **2001**, *17*, 1670. (d) Bronich, T. K.; Nguyen, H. K.; Eidenberg, A.; Kabanov, A. V. *J. Am. Chem. Soc.* **2000**, *122*, 8339. (e) MacKnight, W. J.; Ponomarenko, E. A.; Tirrell, D. A. *Acc. Chem. Res.* **1998**, *31*, 781.

(20) Hong, J. W.; Henme, W. L.; Keller, G. E.; Rinke, M. T.; Bazan, G. C. *Adv. Mater.* **2006**, *18*, 878.

(21) Giachè, V.; Pirami, L.; Becciolini, A. *J. Biolumin. Chemilumin.* **1994**, *9*, 229.

(22) Sambrook, J.; Fritsch, E. F.; Maniatis, T. *Molecular Cloning: A Laboratory Manual*, 2nd ed.; Cold Spring Harbor: New York, 1989; Appendix E.

(23) (a) Rajeevan, M. S.; Ranamukhaarachchi, D. G.; Vernon, S. D.; Unger, E. R. *Methods* **2001**, *25*, 443. (b) Berney, H.; West, J.; Haefele, E.; Alderman, J.; Lane, W.; Collins, J. K. *Sens. Actuators, B* **2000**, *68*, 100.

(24) Cosa, G.; Focsaneanu, K.-S.; McLean, J. R. N.; McNamee, J. P.; Sciano, J. C. *Photochem. Photobiol.* **2001**, *73*, 585.

(25) Schweitzer, C.; Scaiano, J. C. *Phys. Chem. Chem. Phys.* **2003**, *5*, 4911.

(26) Rye, H. S.; Dabora, J. M.; Quesada, M. A.; Mathies, R. A.; Glazer, A. N. *Anal. Biochem.* **1993**, *208*, 144.

(27) Singer, V. L.; Jones, L. J.; Yue, S. T.; Haugland, R. P. *Anal. Biochem.* **1997**, *249*, 228.

(28) Ashley, N.; Harris, D.; Poulton, J. *Exp. Cell Res.* **2005**, *303*, 432.

(29) Gray, G. D.; Wickstrom, E. *Antisense Nucleic Acid Drug Dev.* **1997**, *7*, 133.

(30) Reyderman, L.; Stavchansky, S. *J. Chromatogr., A* **1996**, *755*, 271.

(31) Bontemps, J.; Houssier, C.; Fredericq, E. *Nucleic Acids Res.* **1975**, *2*, 971.

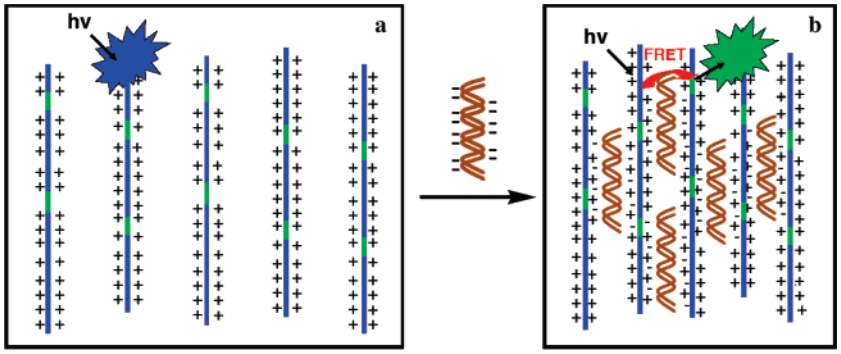

Figure 1. Schematic representation of optical changes induced by complexation of dsDNA with **PFPB$_x$**. (a) Isolated chains of **PFPB$_x$** emit blue light in the absence of DNA. (b) Aggregation with negatively charged dsDNA induces interchain energy transfer to BT sites and changes emission color to green.

Chart 2. Molecular Structures of **poly1$_{10}$** and **poly1$_{20}$**

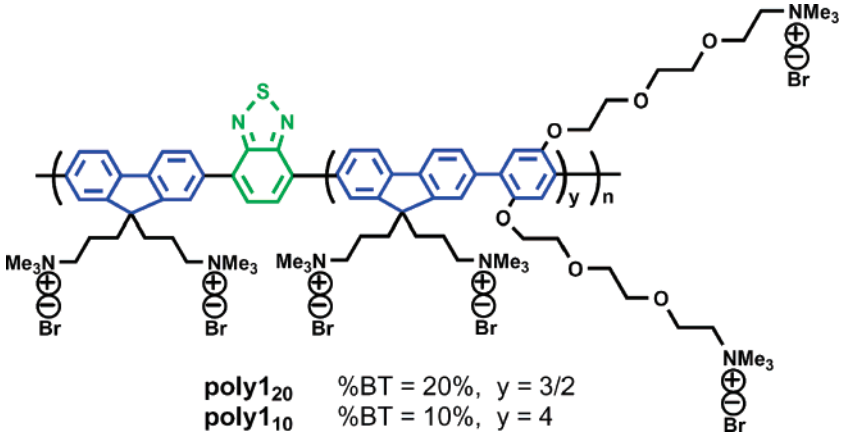

output, and self-quenching. Despite this complexity, we show how that the spectral changes can be treated to yield a parameter δ, which forms the basis for generating calibration curves. The dependence of δ on specific conditions such as the concentrations of the conjugated polyelectrolytes and the dsDNA, type of medium, and conjugated polyelectrolyte composition provides insight into the mechanism of action of the assay and provides the foundation for optimizing the assay so that it is responsive to 7 orders of magnitude differences in [dsDNA].

Results and Discussion

Design, Synthesis, and Characterization of poly1$_{10}$ and poly1$_{20}$. The primary concern for polymer design was to increase substantially the solubility in aqueous media. With this consideration in mind, we chose to synthesize copolymers **poly1$_{10}$** and **poly1$_{20}$**, as shown in Chart 2. Structural elements incorporated to increase solubility include shorter alkyl chains on the fluorene monomers, which reduce the hydrophobic content of the chain,[32] and the introduction of tetralkylammonium units onto the phenylene monomers via oligo(ethylene oxide) segments.[33] Another difference, relative to conjugated polyelectrolytes derived from **PFPB$_x$**, is that the BT sites are flanked by two fluorene repeat units.

Scheme 1 shows the synthetic route to **poly1$_{10}$** and **poly1$_{20}$**. Treatment of 2,7-dibromofluorene (**1**) with 45% KOH aqueous solution, followed by reaction with excess 1,3-dibromopropane, provides 2,7-dibromo-9,9′-bis(3″-bromopropyl)fluorene (**2**) in 85% yield. Compound **2** was transformed into its corresponding boronic ester, 2,7-bis(4,4,5,5-tetramethyl-[1,3,2]-dioxaborolane)-9,9-bis(3′-bromopropyl)fluorene (**3**), by Miyaura reaction in 85% yield.[34] Commercially available 1,4-dibromo-2,5-dihydroxyl benzene (**4**) was treated with 2-[2-(2-chloroethoxy)ethoxy]-ethanol in the presence of K_2CO_3 in DMF at 80 °C to give **5**, in which the hydroxyl groups were then protected by reaction with tosylchloride to afford compound **6**. The tosylate groups in **6** were converted into bromides by treatment with LiBr in refluxing acetone to provide compound **7**. Suzuki cross-coupling copolymerization of **3**, **7**, and 4,7-dibromo-2,1,3-benzothiadiazole (**8**)[14] in the appropriate ratios provides the neutral precursor **poly1$_{10}$N** and **poly1$_{20}$N** in which 10% and 20% of the monomer units are BT, respectively. The BT content is regulated by the ratio of **7** and **8** at the synthesis stage. Since the monomer reactivity ratios are not known for this type of polymerization, we assume a random distribution of monomers throughout the chain. Purification of the precursor materials is accomplished by precipitation of chloroform solutions into methanol three times. In the final step, the neutral polymers are treated with condensed trimethylamine in a THF/methanol mixture. After removal of volatiles, the target cationic species **poly1$_{10}$** and **poly1$_{20}$** were obtained in greater than 90% yields.[35]

(32) Liu, B.; Gaylord, B. S.; Wang, S.; Bazan, G. C. *J. Am. Chem. Soc.* **2003**, *125*, 6705.
(33) (a) Zhou, Q.; Swager, T. M. *J. Am. Chem. Soc.* **1995**, *117*, 12593. (b) Wosnick, J. H.; Mello, C. M.; Swager, T. M. *J. Am. Chem. Soc.* **2005**, *127*, 3400. (c) Marsella, M. J.; Carroll, P. J.; Swager, T. M. *J. Am. Chem. Soc.* **1994**, *116*, 9347. (d) Marsella, M. J.; Carroll, P. J.; Swager, T. M. *J. Am. Chem. Soc.* **1995**, *117*, 9832. (e) Wosnick, J. H.; Liao, J. H.; Swager, T. M. *Macromolecules*, **2005**, *38*, 9287. (f) Zheng, J.; Swager, T. M. *Chem. Commun.* **2004**, 2798. (g) Kim, I. B.; Erdogan, B.; Wilson, J. N.; Bunz, U. H. F. *Chem.—Eur. J.* **2004**, *10*, 6247.
(34) (a) Suzuki, A. *J. Organomet. Chem.* **1999**, *576*, 147. (b) Miyaura, N.; Suzuki, A. *Chem. Rev.* **1995**, *95*, 2457. (c) Jo, J.; Chi, C.; Höger, S.; Wegner, G.; Yoon, D. Y. *Chem.—Eur. J.* **2004**, *10*, 2681.
(35) Liu, B.; Bazan, G. C. *Proc. Natl. Acad. Sci. U.S.A.* **2005**, *102*, 589.

Scheme 1. Synthetic Entry into **poly1$_{10}$** and **poly1$_{20}$**[a]

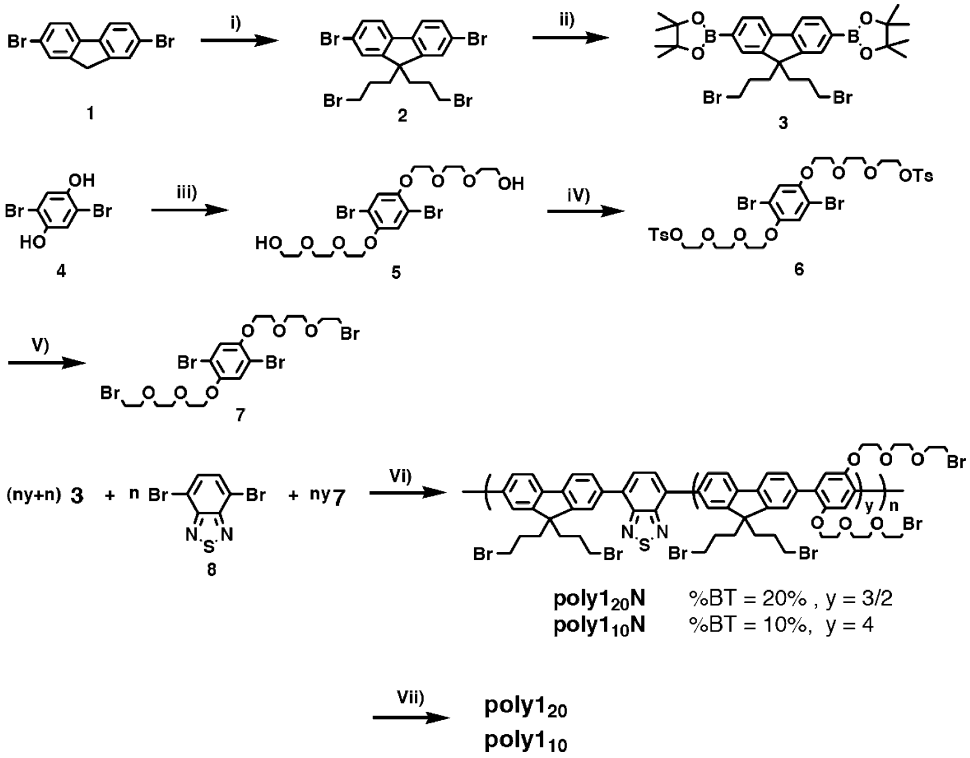

[a] (i) $Br(CH_2)_3Br$, 45% KOH, 80 °C; (ii) bis(pinacolato)diboron, $Pd(dppf)Cl_2$, KOAc, DMSO, 80 °C; (iii) 2-[2-(2-chloroethoxy)ethoxy]ethanol, K_2CO_3, DMF, 80 °C; (iv) TsCl, DMAP, Et_3N, CH_2Cl_2, 0 °C → 25 °C; (v) LiBr, acetone, reflux; (vi) $Pd(PPh_3)_4$, 2 M K_2CO_3, toluene; (vii) $N(CH_3)_3$, THF/H_2O.

Analysis by ^{1}H NMR spectroscopy in d^6-DMSO reveals broad overlapping signals that preclude accurate determination of the degree of quaternization. We relied instead on elemental analysis for confirmation of structure (see Experimental Section). Returning to our goal of increasing water solubility, we estimate that **poly1$_{10}$** and **poly1$_{20}$** display a water solubility of up to 15 mg/mL. For **PFPB$_x$** a similar evaluation is difficult since a small amount of methanol is necessary prior to water addition. It is important to note the different charge densities and water solubilities; **poly1$_{20}$** (or **poly1$_{10}$**) has a positive charge density of 3.2/RU (or 3.6/RU), where RU refers to the average polymer repeat unit,[36] twice that of **PFPB$_7$** (1.7/RU). The increased charge density along the polymer chain is an important additional contributor to the increase in solubility.

UV−vis Absorption and Photoluminescence (PL) Spectra. Providing a baseline understanding of the intrinsic optical properties of the new conjugated polyelectrolytes is necessary prior to looking at the optical changes upon complexation with dsDNA. Figure 2 shows the absorption and photoluminescence (PL) spectra of **poly1$_{10}$** and **poly1$_{20}$** in water and from films obtained by spin coating from methanol. The concentrations of the polymers are provided in terms of RUs. The [RU]s in Figure 2 are 1×10^{-5} M for absorption and 1×10^{-6} M for PL spectra, respectively. The absorption spectra show two bands in the 300−500 nm absorption range (Figure 2a). The band at ∼352 nm is assigned to the π to π^* transition in the fluorene−phenylene segments, while the band located centered near 430 nm is assigned to the BT sites.[37] As the fractional composition of BT in the chain decreases from 20% to 10%, one observes a concomitant reduction of the 430 nm band and a 10 nm red shift of the π to π^* transition. The absorption spectra in the films are red-shifted approximately 10 nm relative to water. Overall, the absorption spectra reflect the composition of the polymer chains with the band at 430 nm increasing in strength as the BT content increases. This last observation will be important when we examine the effect of the PL spectral shapes as a function of polymer concentration.

The PL spectra of **poly1$_{10}$** and **poly1$_{20}$** in water upon excitation at 360 nm are dominated by emission centered at 412 nm (Figure 2b). A broad tail from 500 to 650 nm can be observed in the case of **poly1$_{20}$**. In the films, one observes only green emission and a slightly red-shifted emission maximum for **poly1$_{20}$** (567 nm) relative to **poly1$_{10}$** (541 nm). The solution and solid-state emission spectra are consistent with the idea that less efficient FRET from the phenylene−fluorene segments to the BT sites occurs in isolated chains, relative to situations where interchain energy transfer is possible.

Changes in the PL spectra of **poly1$_{20}$** in water as a function of polymer concentration are shown in Figure 3. These measurements were carried out in a 1 cm × 1 cm cuvette. The

(36) One repeat unit includes one fluorene moiety and relevant content of phenylene and BT. The molecular weight of the RUs are (1 substituted fluorene + 0.6 substituted phenylene + 0.4 BT = 1 × 522.1 + 0.6 × 614.2 + 0.4 × 134.0 = 944.2) 944.2 g/mol and (1 substituted fluorene + 0.8 substituted phenylene + 0.2 BT = 1 × 522.1 + 0.8 × 614.2 + 0.2 × 134.0 = 1040.3) 1040.3 g/mol for **poly1$_{20}$** and **poly1$_{10}$**, respectively.

(37) (a) Bangcuyo, C. G.; Evans, U.; Myrick, M. L.; Bunz, U. H. F. *Macromolecules* **2001**, *34*, 7592. (b) Jayakannan, M.; Van Hal, P. A.; Janssen, R. A. J. *J. Polym. Sci., Part A: Polym. Chem.* **2002**, *40*, 251. (c) Yasuda, T.; Imase, T.; Yamamoto, T. *Macromolecules* **2005**, *38*, 7378. (d) Hou, Q.; Zhou, Q.; Zhang, Y.; Yang, W.; Yang, R. Cao, Y. *Macromolecules* **2004**, *37*, 6299. (e) Herguth, P.; Jiang, X.; Liu, M. S.; Jen, A. K.-Y. *Macromolecules* **2002**, *35*, 6094. (f) Huang, J.; Xu, Y.; Hou, Q.; Yang, W.; Yuan, M.; Cao, Y. *Macromol. Rapid Commun.* **2002**, *23*, 709. (g) Yamamoto, T.; Fang, Q.; Morikita, T. *Macromolecules* **2003**, *36*, 4262. (h) Cadby, A.; Dean, R.; Jones, R. A. L.; Lidzey, D. G. *Adv. Mater.* **2006**, *18*, 2713. (i) Vehse, M.; Liu, B.; Edman, L.; Bazan, G. C.; Heeger, A. J. *Adv. Mater.* **2004**, *16*, 1001.

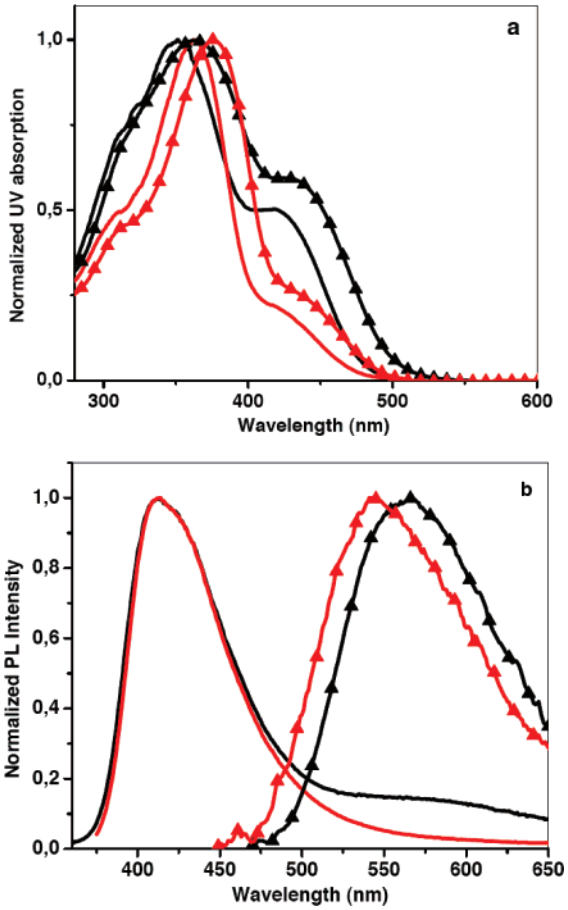

Figure 2. Dependence of absorption and emission spectra as a function of polymer structure in water and in the bulk. (a) UV−vis absorption and (b) PL spectra (λ_{exc} = 360 nm) of **poly1$_{20}$** (black curves) and **poly1$_{10}$** (red curves) in water (solid line) and as thin films (line and triangles). (a) [RU] = 1×10^{-5} M; (b) [RU] = 1×10^{-6} M.

most intense emission is observed when [RU] = 2.0×10^{-5} M. When [RU] < 2.0×10^{-5} M, the intensity decreases without a change in emission maximum or spectral characteristics. Increasing [RU] above 2.0×10^{-5} M also results in a decrease of PL intensity at 414 nm, but a gradual red shift of the emission maximum takes place, together with a change in the general features of the band. Similar behavior is observed with **poly1$_{10}$**. At the higher [RU]s, the spectra cannot be described by a simple sum of the blue and green components. However, the spectral changes can be accommodated by taking into consideration inner filter effects because of the overlap between the emission band and the BT-centered absorption (see Figure 2).

Inspection of how the PL intensity changes as a function of polymer concentration and wavelength should yield additional supporting information on the importance of inner filter effects. Figure 3b provides the change in PL intensity at 414 and 580 nm vs [RU] ([RU] = 7×10^{-8} to 1.0×10^{-3} M). One can observe a decrease of the PL emission at both wavelengths for [RU] > 2.0×10^{-5} M. However, the rate of decrease is more pronounced at 414 nm. These observations are consistent with the idea of a substantial inner effect in the BT absorption region. At 580 nm such absorption is not as significant (Figure 2a), and the decrease in this region of the spectrum may be attributed to self-quenching as a result of polymer aggregation, particularly when [RU] > 8.0×10^{-5} M. Furthermore, when a 0.2 cm × 0.2 cm cuvette was used in an effort to decrease self-absorption,

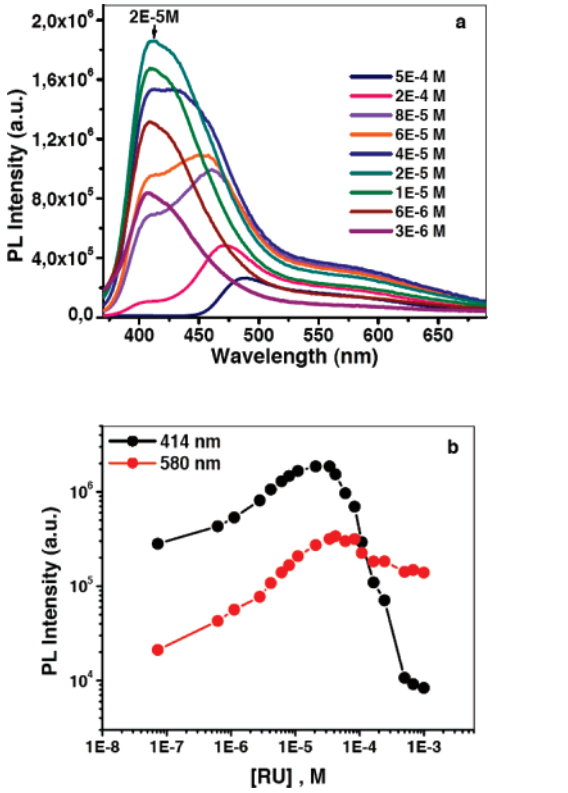

Figure 3. Emission properties of **poly1$_{20}$** in concentrated solutions are modified by inner filter effects. (a) Concentration dependence of the PL spectra of **poly1$_{20}$** (λ_{exc} = 360 nm) in water using a 1 cm × 1 cm cuvette. (b) PL intensity vs [RU] from 7×10^{-8} to 1×10^{-3} M at 414 nm (black) and 580 nm (red).

the most intense emission at 414 nm was found at [RU] = 8×10^{-5} M (see Figure S-1 in the Supporting Information). Self-absorption thus sets an upper limit for [DNA] determination; the exact value is determined by the excitation and emission path lengths and therefore by the dimensions of the cuvette. From a broader perspective, it is informative to compare the threshold [RU]s for **poly1$_{10}$** (2×10^{-5} M) and **poly1$_{20}$** (2×10^{-5} M) to that of **PFPB$_7$** (1×10^{-6} M). The limited solubility of **PFPB$_7$** induces aggregation and green emission after the threshold [RU]. That the PL spectra of **poly1$_{20}$** (or **poly1$_{10}$**) are less perturbed by [RU] relative to **PFPB$_7$** nicely reflects the increased water solubility.

PL Response to dsDNA Addition: Saturation Point. Having established the emission profiles of **poly1$_{10}$** and **poly1$_{20}$** under different conditions provides us with the baseline for understanding perturbations upon complexation with dsDNA. Figure 4a shows the changes in the PL spectra of **poly1$_{20}$** in water ([RU]$_0$ = 2.0×10^{-5} M; [RU]$_0$ corresponds to the initial polymer concentration prior to dsDNA addition) upon addition of dsDNA in increments of 1×10^{-6} M ([dsDNA] will be reported relative to bps throughout the paper) up to a concentration of 1.8×10^{-5} M bps. The dsDNA used in all the studies is 30 bps long. A distinguishing feature of the PL spectra is that as [dsDNA] increases, the intensity of the green emission band grows at the expense of the blue emission, via an apparent isosbestic point at 485 nm. During the evolution of PL spectra shown in Figure 4a, the [RU] decreases from 2×10^{-5} M to 1.35×10^{-5} M due to dilution by addition of dsDNA. Changes in the PL spectra saturate when [dsDNA] = 1.6×10^{-5} M. Under these conditions [RU]/[dsDNA] ≈ 0.9 and the ratio of

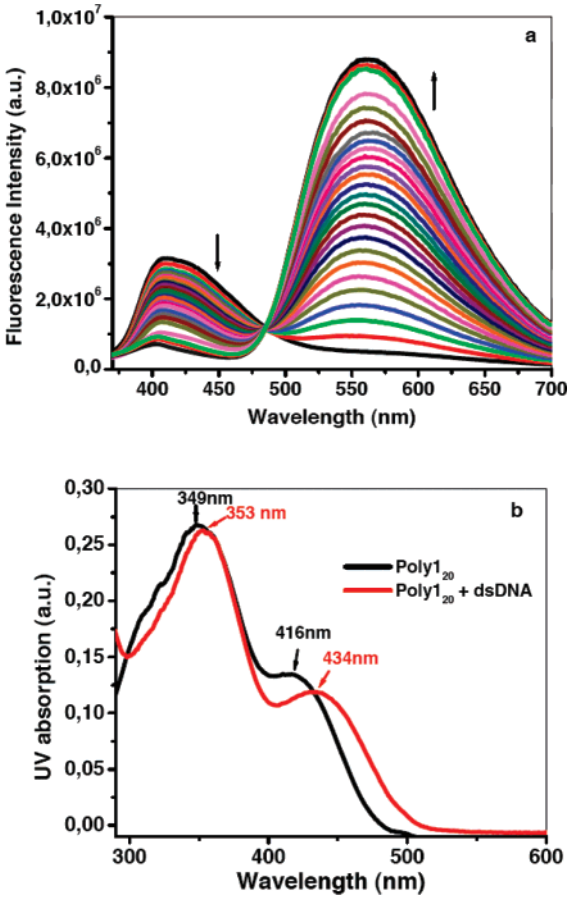

Figure 4. Emission of **poly1$_{20}$** is red-shifted and increases in intensity upon complexation with dsDNA. (a) PL spectra ($\lambda_{exc} = 360$ nm) of **poly1$_{20}$** ([RU]$_0$ $= 2.0 \times 10^{-5}$ M) with 32 μL additions of 5.0×10^{-5} M of 30 bp dsDNA. The [dsDNA] range spans from 0 to 1.8×10^{-5} M. (b) UV−visible absorption spectra of **poly1$_{20}$** ([RU] $= 2.0 \times 10^{-5}$ M) and **poly1$_{20}$**/dsDNA complexes in water ([RU] $= 2.0 \times 10^{-5}$ M and [dsDNA] $= 1.6 \times 10^{-5}$ M).

the negative charge to positive charge ($R_{-/+}$) is approximately 0.7. The absorption spectra of **poly1$_{20}$** ([RU] $= 2 \times 10^{-5}$ M) in the absence and presence dsDNA (1.6×10^{-5} M) given in Figure 4b show a red shift of ~5 nm for the $\pi \rightarrow \pi^*$ transition band and of ~15 nm at longer wavelengths, indicating the new environment upon complexation with dsDNA. The changes observed in the PL spectra are similar when using **poly1$_{10}$**.

We now dissect the spectral evolution in Figure 4a into independent contributions from changes of the BT emission output, the FRET efficiency, and emission self-quenching of the polymer itself. We approach the problem of BT output by exciting the solutions at the two [dsDNA] extremes in Figure 4a at 451 nm and measuring the resulting PL spectra. This excitation wavelength results in identical absorbance values and corresponds to direct BT excitation. These experiments show that the PL intensity of BT is approximately 11 times stronger when in the presence of the dsDNA. Under the same conditions, but exciting at 360 nm, where excitation of the phenylene−fluorene segments occurs, one finds an 18-fold increase in BT emission. Thus, we can estimate that the FRET efficiency in the presence of dsDNA increases by a factor of approximately 1.6. It is also significant that the emission of the parent BT-free polymer, i.e., **poly1$_0$**, is also quenched upon dsDNA complexation (see Figure S-2 in the Supporting Information). For example, addition of 1.6×10^{-5} M dsDNA results in a

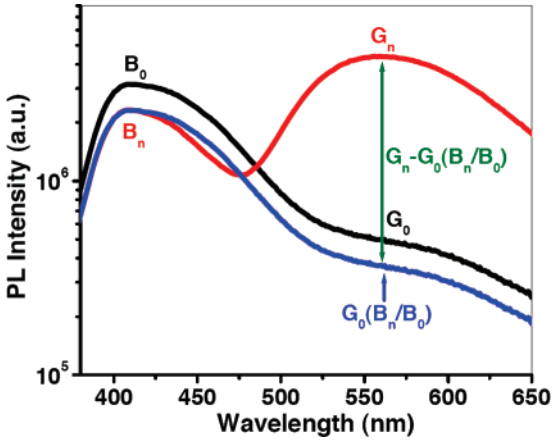

Figure 5. Method for using PL spectra to calculate δ using eq 1. The black and red curves correspond to the emission of **poly1$_{20}$** in the absence of dsDNA and after the nth addition of dsDNA, respectively. The blue curve is the normalized spectra of the black curve at 414 nm. The curves were extracted from Figure 4; the [dsDNA] is 8.8×10^{-6} M for the red curve.

30% decrease in the PL intensity of **poly1$_0$**. Thus, even though there is a well-defined isosbestic point in Figure 4, several concurrent processes are taking place: the FRET efficiency increases, the BT PL quantum yield increases, and there is partial quenching of the phenylene−fluorene segments.

Despite the complex mix of optical processes involved in Figure 4a, quantitative information on how the PL spectra correlate with [dsDNA] can be obtained via the dimensionless parameter δ, defined in eq 1:

$$\delta = \frac{G_n - G_0\left(\frac{B_n}{B_0}\right)}{N} \qquad (1)$$

where G_0 and G_n are the integrated (green) fluorescene in the range of 520 to 660 nm in the absence of dsDNA and after the nth addition of dsDNA, respectively; B_0 and B_n are the integrated (blue) fluorescence in the 375−470 nm range in the absence and after the nth addition of dsDNA, respectively; N is a normalization factor, obtained in our case by using the integrated emission of **poly1$_{20}$** in the 375 to 470 nm range at [RU] $= 1.0 \times 10^{-6}$ M, which was used for all δ determinations. Including N allows comparison of measurements from different instruments and optical collection conditions thereby greatly simplifying data analysis. An illustration of how to extract δ from PL spectra is shown in Figure 5, where the emission in the absence of dsDNA (black curve) is normalized at 414 nm relative to the spectrum obtained after the nth addition of dsDNA (red curve). We note here that the apparent spectral dissimilarity between Figure 5 and Figure 4a is due to the fact that we chose a semilogarithmic scale for the PL intensity in Figure 5. This choice was made to better highlight the differences between G_0 and G_n. With the normalized emission spectrum (blue curve) one can extract $G_0(B_n/B_0)$. The increase of the integrated green emission as a result of dsDNA addition is obtained from $G_n - G_0(B_n/B_0)$, which is proportional to δ. It is also worth emphasizing that eq 1 was obtained empirically and is based on the anticipation that the increase of the green band would be proportional to the fraction of polymer chains that are complexed to dsDNA.

Probing the effect of the initial conjugated poyelectrolyte/dsDNA stoichiometric ratio is relevant because the resulting aggregate structures can, under certain circumstances, be

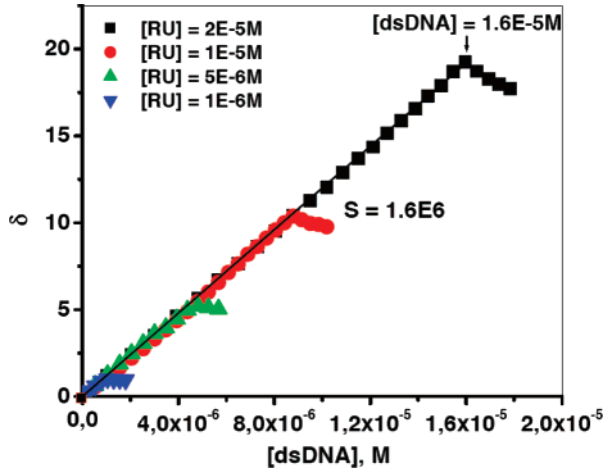

Figure 6. Different polymer concentrations show overlap in the response plots of δ vs [dsDNA] for 30 bp dsDNA and **poly1$_{20}$** at $[RU]_0 = 1 \times 10^{-6}$ M (blue), 5×10^{-6} M (green), 1×10^{-5} M (red), 2×10^{-5} M (black).

Table 1. Slopes of δ vs [dsDNA] Plots in Different [dsDNA] Ranges

[dsDNA] range[a] (M)	slope (M^{-1})
8.0×10^{-7} to 1.3×10^{-7}	1.6×10^{6}
2.0×10^{-9} to 3.3×10^{-10}	2.1×10^{7}
2.4×10^{-10} to 6.0×10^{-11}	1.7×10^{8}
3.0×10^{-11} to 5.0×10^{-12}	1.7×10^{9}

[a] $[RU]_0 = 1 \times 10^{-6}$ M.

controlled by kinetic effects.[38] Figure 6 provides the δ response to dsDNA at four different initial polymer concentrations ($[RU]_0 = 1.0 \times 10^{-6}$, 5.0×10^{-6}, 1.0×10^{-5}, 2.0×10^{-5} M). We did not examine conditions when $[RU]_0 > 2 \times 10^{-5}$ M due to the inner filter effect and the resulting distortions in the PL spectra shown in Figure 3. Figure 6 shows that there is a linear increase of δ vs [dsDNA] up to a critical [dsDNA] value, after which one observes a *decrease* of δ. The point of critical [dsDNA] depends on the original concentration of the polyelectrolyte. For example, when $[RU]_0 = 2.0 \times 10^{-5}$ M, the point at which δ begins to decrease occurs at [dsDNA] $= 1.6 \times 10^{-5}$ M. A similar linear dependence of δ vs [dsDNA] is observed for the lower $[RU]_0$s, except that the critical [dsDNA] is lower. Regardless of $[RU]_0$, the saturation limit occurs when $[RU]_0$/[dsDNA] is approximately 0.9; under these circumstances the ratio of negative to positive charges ($R_{-/+}$) is approximately 0.7. Such a constant ratio indicates a stoichiometric limit for the polyelectrolyte complex. From a practical perspective, the saturation point provides the limit for the proportional correlation between δ and [dsDNA] at higher concentrations. That the slopes in the δ vs [dsDNA] plots are insensitive to $[RU]_0$ will have significant ramifications later when we incorporate the response of two initial polymer concentrations to attain a sensitive response across a wide [dsDNA] range.

Examination of the Lower [dsDNA] Limit. We turn our attention in this section on what happens at very low [dsDNA] to determine the lower limit of the δ response. Lower [dsDNA] regimes were studied by using solutions of **poly1$_{20}$** at a constant initial concentration ($[RU]_0 = 1 \times 10^{-6}$ M), and the results are summarized in Table 1. Four specific [dsDNA] ranges were probed (in M bps: 1.3×10^{-7} to 8×10^{-7}, 3.3×10^{-10} to 2×10^{-9}, 6×10^{-11} to 2.4×10^{-10}, and 5×10^{-12} to 3×10^{-11}) by adding 5 μL aliquots of stock solutions with concentrations of 5×10^{-5}, 1×10^{-7}, 1.8×10^{-8}, and 1.6×10^{-9} M bps, respectively. Plots of δ vs [dsDNA] are linear within each concentration range, with each plot consisting of at least six independent measurements. Figure 7 shows the result for the lowest concentration range. Comparison of Figures 7b and 4 highlights that only minor changes occur in the PL spectra at low concentrations and illustrates the low δ values obtained with small quantities of dsDNA. Plots of δ vs [dsDNA] with [dsDNA] $< 5 \times 10^{-12}$ M were not linear; the data were scattered. Thus, the lower limit for the assay under these experimental conditions is close to [dsDNA] $= 5 \times 10^{-12}$ M.

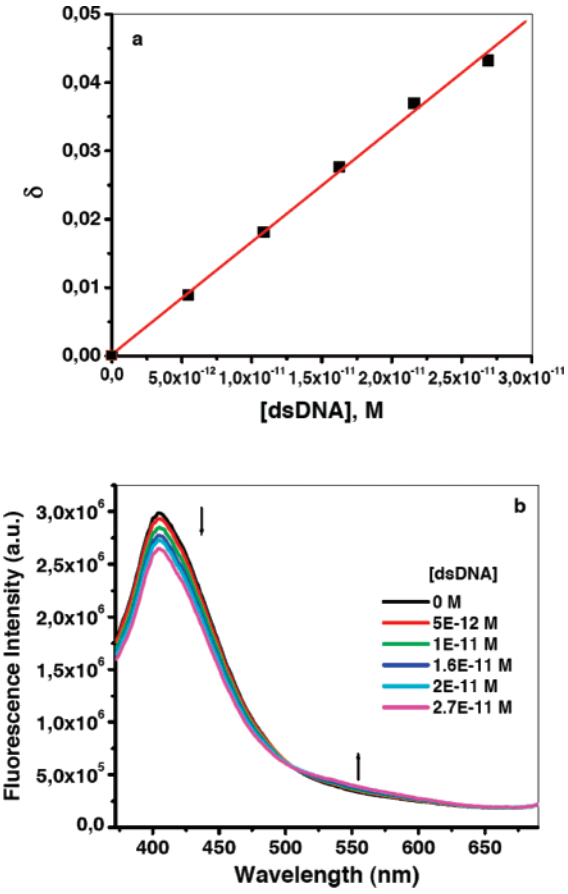

Figure 7. Change in PL spectra and δ are minor when **poly1$_{20}$** is in large excess. (a) Plot of δ as a function of [dsDNA] in the concentration range of 5×10^{-12} to 3×10^{-11} M; (b) PL spectra of **poly1$_{20}$** ($[RU]_0 = 1 \times 10^{-6}$ M) with 5 μL additions of 1.6×10^{-9} M of [dsDNA] ($\lambda_{exc} = 360$ nm).

Examination of Table 1 shows that the slopes of linear plots are not equal in the different concentration regimes. There is a progressive increase in slope with decreasing [dsDNA], from 2.1×10^{7} M^{-1} ([dsDNA] $= 2.0 \times 10^{-9}$ M to 3.3×10^{-10} M) to 1.7×10^{9} M^{-1} ([dsDNA] $= 3.0 \times 10^{-11}$ M to 5.0×10^{-12} M). At the higher concentrations in Figure 6, the slope is 1.6×10^{6} M^{-1}. Therefore, the proportionality constant between δ and [dsDNA] changes when one examines very wide concentration ranges. A direct consequence is that extrapolation is not reliable and δ vs [dsDNA] calibration curves thus need to be established.

Examination of PL Response across a Broad [dsDNA] Range. We now examine the behavior of δ throughout a broad

(38) Wang, S.; Bazan, G. C. *Chem. Commun.* **2004**, 2508.
(39) Israelachvili, J. *Intermolecular & Surface Forces*; Academic Press: London, 1992.
(40) Wang, F.; Bazan, G. C. *J. Am. Chem. Soc.* **2006**, *128*, 15786.

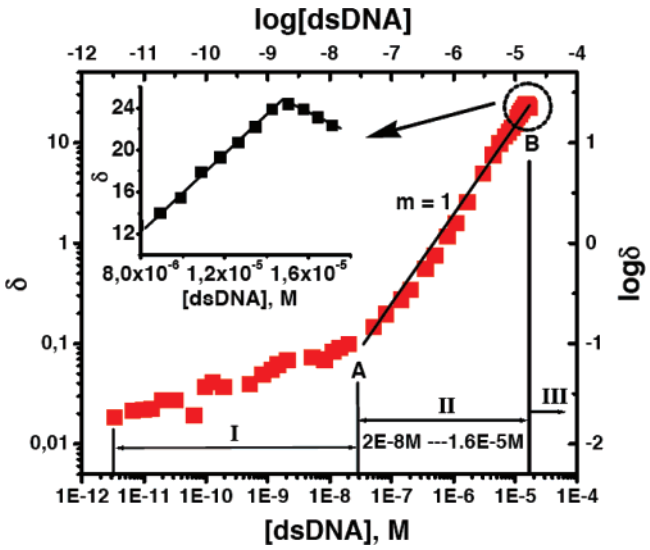

Figure 8. δ response across a wide [dsDNA] range reveals three regimes and two inflection points. Plot of δ vs [dsDNA] in the concentration range 3×10^{-12} to 2.1×10^{-5} M. The $[RU]_0$ of **poly1$_{20}$** is at 2×10^{-5} M. The inset shows the linear plot of δ vs [dsDNA], with [dsDNA] from 8.0×10^{-6} to 1.8×10^{-5} M.

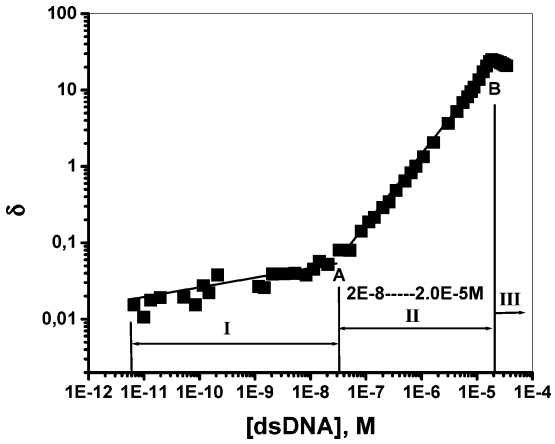

Figure 9. Plot of δ vs [dsDNA] in the concentration range 3×10^{-12} to 3×10^{-5} M using a double logarithmic scale. The $[RU]_0$ of **poly1$_{10}$** is at 2×10^{-5} M.

[dsDNA] range. The experiments were done with **poly1$_{20}$** at $[RU]_0 = 2 \times 10^{-5}$ M. Stock solutions of dsDNA with different concentrations were prepared and then added in appropriate volumes to the polymer solution in order to cover a [dsDNA] range from 3×10^{-12} to 2.1×10^{-5} M. The results are shown in Figure 8, where δ vs [dsDNA] is plotted using a double logarithmic scale. The plot in Figure 8 can be broken down into three regimes, labeled "I", "II", and "III", with inflection points "A" and "B". In regime "I", where [dsDNA] increases from 3×10^{-12} to 2×10^{-8} M, the blue component of the PL spectra decreases slightly and there are negligible changes in the green component (Figure S-3a). The slope using the double logarithmic scale is less than 1. From 2×10^{-8} to 1.6×10^{-5} M, i.e., regime "II", the changes in PL spectra are more significant and are similar to those shown in Figure 4 (see Figure S-3b). Here the decrease in blue emission is accompanied by a rapid increase of green emission. In Figure 8, the slope in this [dsDNA] range is approximately 1. In the "III" regime, i.e., after the saturation limit, the blue emission remains relatively constant and the green band decreases, possibly due to self-quenching in the aggregated state (see inset of Figure 8 and Figure S-3c). In Figure 8, the "A" turning point, where one kind of responsive regime changes to another one, occurs at 2×10^{-8} M. "B" is the previously discussed stoichiometric limit for these polyelectrolyte complexes, which occurs at 1.6×10^{-5} M and sets the upper limit for measuring [dsDNA].

Comparison of poly1$_{10}$ and poly1$_{20}$. Comparison of the δ vs [dsDNA] plots using **poly1$_{10}$** and **poly1$_{20}$** allows us to look into how the polymer structure influences the sensitivity of the overall assay. We examined the entire [dsDNA] range measurement with **poly1$_{10}$**, and the results of this study are shown in Figure 9. From these data one observes that the overall response of **poly1$_{10}$** is similar to that of **poly1$_{20}$**; the three regimes "I", "II", "III" and the two turning points "A", "B" are contained in the plot. Turning point "A" at 2×10^{-8} M is similar to that observed with **poly1$_{20}$**. The upper limit set by "B" is at 1.9×10^{-5} M, which is slightly higher than that of **poly1$_{20}$** (1.6×10^{-5} M), perhaps as a result of the higher charge density per average RU of **poly1$_{10}$**. It should be noted, however, that the plot in the linear scale shows that **poly1$_{20}$** has a steeper slope ($m = 1.6 \times 10^6$ M^{-1}) than **poly1$_{10}$** ($m = 1.3 \times 10^6$ M^{-1}) between [dsDNA] $= 2 \times 10^{-8}$ M bps and 1.6×10^{-5} M bps, thus providing higher sensitivity (see Figure S-4 in the Supporting Information).

Effect of $[RU]_0$ in the Low [dsDNA] Regime. One observes from Figure 6 that the high concentration response limit of δ is determined by point "B" and therefore by $[RU]_0$. However, starting with $[RU]_0 = 2.0 \times 10^{-5}$ M, the $R_{-/+}$ in the "I" regime of Figures 8 or 9 is small, from 1.9×10^{-7} to 1.3×10^{-3}. In other words, there is a very large excess of conjugated polyelectrolyte relative to dsDNA. The result is unsurprising; only minor perturbations in the PL spectra are observed since most of the conjugated polymer chains remain in their original state (see Figure S-3a in the Supporting Information for **poly1$_{20}$**). Under the conditions where there is a large excess of polymer, $G_n \approx G_0$ and $B_n \approx B_0$. From eq 1, one sees that a small change in δ would be expected. Lowering $[RU]_0$ was anticipated to provide a more sensitive response, since when a larger fraction of polymer chains are complexed to dsDNA, then $G_n > G_0$ and $B_n < B_0$. For studying the low concentration regimes, we focused on **poly1$_{10}$** because its higher PL quantum efficiency in water ($4 \pm 1\%$) relative to that of **poly1$_{20}$** ($1 \pm 0.4\%$) was expected to provide better signal-to-noise.

Figure 10 allows for a comparison of the changes in the PL spectra of **poly1$_{10}$** at different $[RU]_0$s (in M: 2×10^{-5}, 1×10^{-6}, and 2×10^{-7}) upon addition of similar dsDNA quantities (from 3×10^{-12} to 2×10^{-7} M). For ease of comparison the PL spectra were normalized relative to the intensity in the absence of dsDNA. When the polymer concentration is highest ($[RU] = 2 \times 10^{-5}$ M, Figure 10a), the blue component of the spectra changes by ~2%, with negligible perturbation in the green region. In the intermediate situation, Figure 10b, the decrease of blue emission accompanied by the increase of green emission becomes easily detectable. The largest spectral changes are observed when the polymer concentration is most dilute, as in Figure 10c. The collective set of observations indicates that the assay sensitivity when [dsDNA] $< 2 \times 10^{-8}$ M depends on $[RU]_0$. However, when $[RU]_0 < 1 \times 10^{-7}$ M the polymer emission becomes too weak to measure reliably using our fluorometer and sets the lower limit threshold.

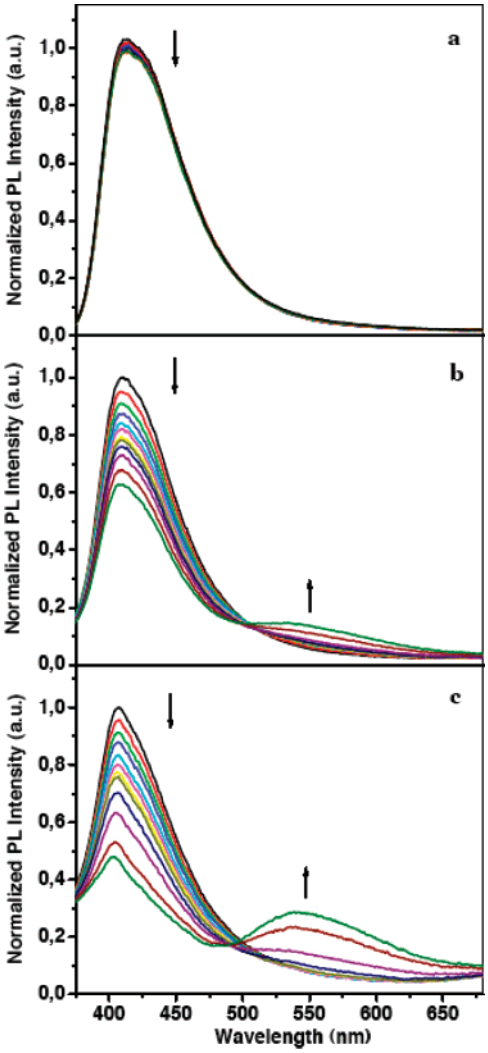

Figure 10. Larger changes in emission take place when the excess of **poly1$_{10}$** relative to dsDNA decreases. PL spectra of **poly1$_{10}$** after additions of dsDNA (λ_{exc} = 360 nm). The $[RU]_0$s of **poly1$_{10}$** are (a) 2×10^{-5} M; (b) 1×10^{-6} M, and (c) 2×10^{-7} M, respectively. For all of the cases, the [dsDNA] ranges from 3×10^{-12} to 2×10^{-7} M. For ease of comparison, the initial PL intensities in the absence of dsDNA were normalized.

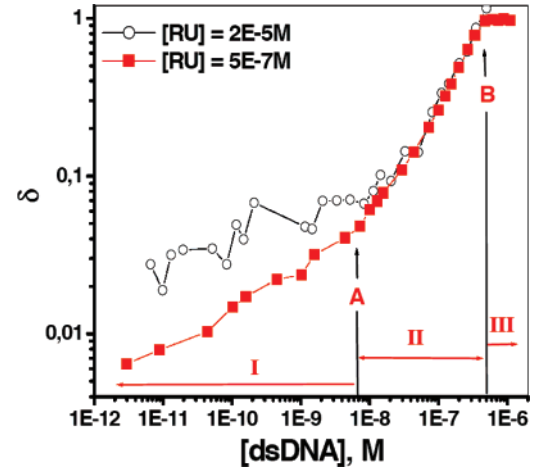

Figure 11. Plots of δ as a function of [dsDNA] using a double logarithmic scale reveal less scatter with lower **poly1$_{10}$** concentrations. The $[RU]_0$s of **poly1$_{10}$** are 2×10^{-5} M (black curve) and 5×10^{-7} M (red curve).

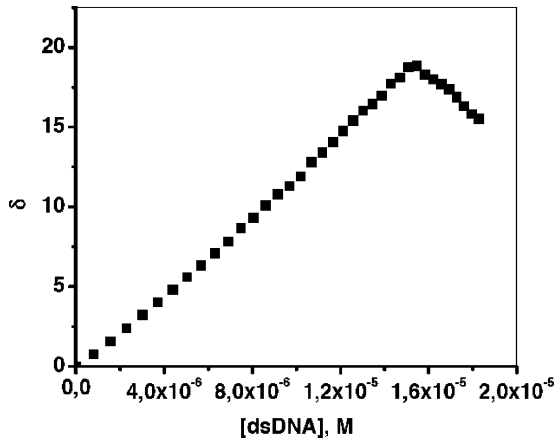

Figure 12. Plot of δ vs [dsDNA] in 25 mmol phosphate buffer (pH = 7.4) for **poly1$_{20}$** ($[RU]_0 = 2 \times 10^{-5}$ M) shows a similar response to that obtained in water (see Figure 6).

Further fine-tuning of the **poly1$_{10}$** $[RU]_0$ was undertaken to obtain optimal performance. In these experiments the δ response was measured with $[RU]_0 = 1 \times 10^{-6}$, 5×10^{-7}, 2×10^{-7}, and 1×10^{-7} M. The least data scatter and steepest slope were observed with $[RU]_0 = 5 \times 10^{-7}$ M, as shown in Figure 11. The corresponding plots for $[RU]_0 = 2 \times 10^{-7}$ and 1×10^{-7} M were deposited as Figure S-5 in the Supporting Information. In Figure 11, the saturation limit occurs when [dsDNA] = 5×10^{-7} M. For comparison, the plot obtained with $[RU]_0 = 2 \times 10^{-5}$ M is also included in Figure 11. When comparing the two different concentrations, one notes that, with $[RU]_0 = 5 \times 10^{-7}$ M, the δ values change more quickly and are less scattered in the "I" regime and the "A" point occurs at a lower [dsDNA] (6×10^{-9} M), although this transition is not as clearly defined. The sensitivity and reliability of the assay therefore increases when $[RU]_0 = 5 \times 10^{-7}$ M. Significantly, in regime "II", the δ responses from the two $[RU]_0$s in Figure 11, become nearly identical, in agreement with the results in Figure 6.

Effect of Buffer. DNA is more commonly stored in buffered solutions than in pure water. The buffer ions screen negative charges on complementary single-stranded DNA, which facilitates hybridization. However, the same ions are expected to weaken the electrostatic interactions between the positively charged polyelectrolytes and dsDNA. This is often referred to as electrostatic screening, since the external ions decrease, or collapse, the electrostatic interaction of counterions resulting in a decrease in the potential between the two oppositely charged pseudo surfaces.[39] With these considerations in mind, we tested the optical response of **poly1$_{10}$** and **poly1$_{20}$** to dsDNA in 25 mmol of phosphate buffer (pH = 7.4), conditions typical of DNA detection schemes. Addition of dsDNA to either **poly1$_{10}$** or **poly1$_{20}$** gives rise to changes in the PL spectra that are very similar to those shown in Figure 4 (see Figure S-6 in the Supporting Information). A typical plot of δ vs [dsDNA] for **poly1$_{20}$** with $[RU]_0 = 2 \times 10^{-5}$ M is shown in Figure 12. Comparison against the analogous information obtained in water (Figure 6) shows that the slopes of the plots are indistinguishable. The saturation points are at [dsDNA] = 1.6×10^{-5} and 1.5×10^{-5} M in water and buffer, respectively. Thus, the presence of buffer ions makes only a minor modification of the assay response. Such behavior is interesting in view of the expected screening of electrostatic attraction. That this is not the case suggests that the cooperative action of multiple charges in the macromolecules can overcome changes in electrostatic

attraction, at least with the concentration of ion in the buffer used in these experiments.

Summary Discussion and Conclusion

A new class of BT-containing conjugated polyelectrolyte structures is now accessible via the synthetic sequence shown in Scheme 1. The BT content in these copolymers can be modulated at the synthesis stage by controlling the ratio of reacting monomers. These polymers display a much higher water solubility, when compared to polymers such as **PFBT$_7$**, as a result of the higher density of tetralkylammonium groups along the polymer chain and the oligo(ethyleneoxide) pendant groups on the phenylene units. Additionally, the shorter propyl linkers on the fluorene units reduce the hydrophobic content of the polymer.[32]

There is a reduced tendency for the BT-centered green emission band in **poly1$_{10}$** and **poly1$_{20}$** to appear in concentrated aqueous solutions. Films of the materials, where interchain contacts are maximized, emit predominantly green. These data suggest that the increased solubility reduces aggregation, when compared to systems such as **PFBT$_7$**. The PL emission changes as a function of concentration, predominantly as a result of self-absorption of the blue band by the BT chromophores. The exact value for the "maximum" concentration after which distortions in spectral shape are observed thus depends on the dimensions of the cuvette, with smaller volumes allowing one to reach higher concentrations.

Addition of dsDNA to **poly1$_{10}$** or **poly1$_{20}$** causes a decrease in the blue band and an increase of the green emission. These changes are a result of increased energy transfer from the blue emitting regions to BT-centered sites, an increase in the BT emission efficiency and partial quenching of the blue band. The increase in BT quantum yield is likely a result of more effective shielding from water when in the polymer/dsDNA aggregate. Similar observations have recently been reported with anionic BT-containing polyelectrolytes that aggregate at low pH values.[40] In these systems the BT quantum yield exhibits a 7-fold increase when the pH changes from 7 to 3. The overall increase in FRET efficiency throughout the process in Figure 4a is not very large, approximately 1.6, although this is an estimate since the degree of self-quenching of the blue emitting segments is not well-defined at this point. Having identified the complexity of the process involved in producing the changes in PL characteristics, it is remarkable that a linear relationship between δ and [dsDNA] is observed in Figure 6 and that the slope is independent of the polyelectrolyte concentration. We reemphasize that eq 1 was developed empirically on the expectation that increases in green emission would be proportional to the quantity of polyelectrolyte complexed to dsDNA. For all $[RU]_0$s, the increase of δ with increasing [dsDNA] breaks down when the ratio of negative to positive charges is approximately 0.7. Such a consistent value suggests that more of the conjugated polyelectrolyte is incorporated into the aggregate than dsDNA. Possible reasons for the nonequivalent ratio include noncommensurate aspect ratios of the polymer repeat units and the base pairs in dsDNA. Furthermore, it is known that under certain circumstances the aggregate structures are determined under kinetic conditions.[38] Structural details of these aggregates are not available and will be difficult to obtain, particularly at the lowest concentrations where poor signal-to-noise ratios are expected in standard dynamic light scattering experiments.

It is also interesting to note that two slopes are observed in the double logarithmic plots in Figures 8 and 9. These slopes are proportional to the power dependence of δ on [dsDNA]. We assume that δ is proportional to the quantity of **poly1$_{10}$** (or **poly1$_{20}$**) incorporated into the polyelectrolyte aggregate. Under the assumption that the slope equals 1 in regime II suggests that the equilibrium constant for aggregate formation is proportional to [dsDNA]. In the low concentration regime, i.e., I, that the slope < 1 would indicate that a single chain of dsDNA brings in together more polymer chains into the aggregate when the polymer is in much greater excess. The stochiometry of the complex is thus dependent on [dsDNA] at a given [RU]. Such a result is not surprising when one takes into consideration that, in regime I, the charge ratio of dsDNA to CPE ranges from 1.9×10^{-7} to 1.3×10^{-3} starting with $[RU]_0 = 2 \times 10^{-5}$ M. Furthermore, one notices a steeper dependence of the δ vs [dsDNA] plots summarized in Table 1 when one examines lower dsDNA concentrations, consistent with the arguments above.

Despite gaps in our mechanistic understanding in how the combined optical processes come together to determine δ and the general description of the polyelectrolyte aggregates, it is possible to collect the information obtained thus far and to generate calibration curves that may be of practical value for determining [dsDNA]. We highlight that **poly1$_{20}$** has a slightly higher sensitivity than **poly1$_{10}$** in the high [dsDNA] regime. However, because of its intrinsic higher PL quantum efficiency, **poly1$_{10}$** provides better signal-to-noise at lower [dsDNA]. Combining the overall set of observations, we collect in Figure 13 the δ response obtained with **poly1$_{10}$** starting with two different $[RU]_0$s (5×10^{-7} M and 2×10^{-5} M) in either water or buffer solution to generate calibration curves that span a 7 orders of magnitude difference in [dsDNA]. With $[RU]_0 = 5 \times 10^{-7}$ M, we obtain good sensitivity and reproducibility in the low [dsDNA] regime (red curves in Figure 13). Higher [dsDNA]s (black curves) can be interrogated with $[RU]_0 = 2 \times 10^{-5}$ M because the upper "stoichiometric" limit of the polyelectrolyte aggregates increases with higher initial polymer concentrations (see Figure 6). That the dependence of δ is not dependent on [RU] in the intermediate [dsDNA] ranges allows overlap between the curves obtained at different $[RU]_0$s. Figure 13 shows high sensitivity and a wide detectable range. Additionally, based on previous observations with **PFBT$_x$**, we anticipate that similar curves can be provided to quantify ssDNA.[20]

It is useful to point out that the low [dsDNA] range in the plots of Figure 13 is competitive with what can be accomplished with current commercially available technologies based on cyanine dyes such as PicoGreen and OliGreen.[24−31,41] The [dsDNA] ranges in Figure 13 also extend into regions that can be addressed by absorption spectroscopy. One difference between intercalator-based methods and that described here is that the former can correlate [dsDNA] with the emission intensity at a single wavelength. The calibration curves in Figure 13 require analysis of the spectral shapes. To the best of our knowledge, PicoGreen is one of the most sensitive probes.[42] The detection range is from 3.0×10^{-11} M bps, or 25 pg/mL, to 1.5×10^{-6} M bps, or 1 μg/mL. These concentrations span approximately 5 orders of magnitude. By using a normal

(41) http://probes.invitrogen.com/handbook/sections/0803.html.
(42) Singer, V. L.; Jones, L. J.; Yue, S. T.; Haugland, R. P. *Anal. Biochem.* **1997**, *249*, 228.

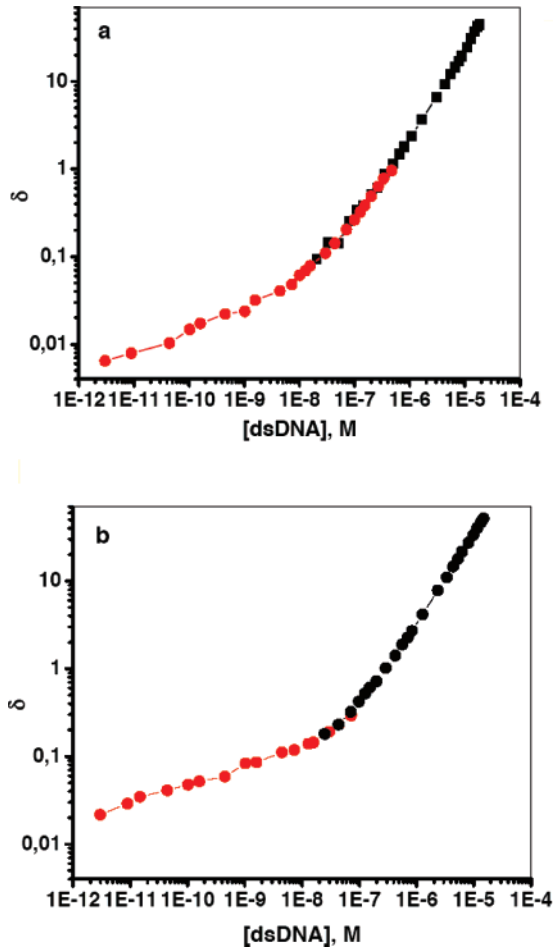

Figure 13. Composite calibration curve of δ vs [dsDNA] using a double logarithmic scale in (a) water and (b) 25 mM phosphate buffer. The concentrations of **poly1$_{10}$** are $[RU]_0 = 2 \times 10^{-5}$ M (black curve) and 5×10^{-7} M (red curve).

fluorometer, as in the conditions of our work, one can use TOTO to probe from 0.5 ng/mL to 100 ng/mL.[43] Other intercalating dyes include OliGreen with a detection range from 3×10^{-10} M, or 100 pg/mL, to 3.0×10^{-6} M, or 1 μg/mL (for single-stranded DNA),[41] i.e., 4 orders of magnitude, and ethidium bromide, which is typically used with concentrations of 1 ng/mL. For comparison, the conjugated polymer assay spans from 3.0×10^{-12} M, or 2 pg/mL, to 1.5×10^{-5} M, or 10 μg/mL, i.e., close to 7 (exactly 6.9) orders of magnitude differences and does not benefit from the extensive prior optimization and mechanistic understanding of intercalating dyes.[44]

Experimental Section

General Details. ^{1}H and ^{13}C NMR spectra were collected on Varian Inova 400 MHz and Varian ASM-100 200 MHz spectrometers. UV−vis absorption spectra were recorded on a Shimadzu UV-2401 PC diode array spectrometer. Photoluminescence spectra were obtained on a Spex Fluorolog 2 spectrometer, using 90° angle detection for solution samples. Mass spectrometry and elemental analysis were performed by the UCSB Mass Spectrometry Lab and Elemental Analysis Center. Reagents were obtained from Aldrich Co. and used as received unless otherwise mentioned. The synthesis of 4,7-dibromo-2,1,3-benzothiadiazole (**8**) was described previously.[14]

All the DNA concentration determination experiments were done by using 30 base pair double-stranded DNA. The sequence of dsDNA was 5′-CTG TTG CAC TAT GCC AGA CAA TAA TTT TCT-3′ with its complementary strand 5′-AGA AAA TTA TTG TCT GGC ATA GTG CAA CAG-3′. HPLC-purified oligonucleotides were obtained from Integrated dsDNA Technologies, Inc. The samples were prepared by initially determining ssDNA strand concentrations based on the absorbance at 260 nm in 300 μL quartz cells using a Beckman Coulter DU800 spectrophotometer. Once the concentration of both strands was established, a 1:1 ratio between complementary single strands was mixed for annealing. The mixture of complementary strands was annealed at 55.8 °C (2 °C below the melting point) for 25 min and then was slowly cooled to room temperature; the absorbance of the hybridized strands was then measured to determine the concentration. The extent of hybridization was checked by variable temperature absorbance spectroscopy. Water was distilled and deionized by using a Millipore filtration system. Measurements in buffer were made using commercially available 25 mmol potassium phosphate monobasic-sodium hydroxide buffer (pH = 7.4) from Fisher Scientific. Fluorescence intensities were determined from the integrated areas under both blue (375−470 nm) and green emission (520−660 nm) bands of emission spectra. In all of the cases, the calibration factor N in eq 1 was obtained by the integration of blue emission from 375 to 470 nm from a solution of **poly1$_{20}$** at [RU] = 1×10^{-6} M in water. The [dsDNA] is provided in terms of base pairs (bps) throughout the paper.

2,7-Dibromo-9,9′-bis(3′′-bromopropyl)fluorene (2). 2,7-Dibromofluorene (15 g, 46.3 mmol) was added to a mixture of aqueous potassium hydroxide (300 mL, 50%), tetrabutylammonium bromide (3.1 g, 9.3 mmol), and 1,3-dibromopropane (93 g, 460 mmol) at 75 °C. After 30 min, the mixture was cooled to room temperature. After extraction with CH_2Cl_2, the combined organic layers were washed successively with water, aqueous HCl (1 M), water, and brine and were then dried over $MgSO_4$. After removal of the solvent and the excess 1,3-dibromopropane, the residue was purified by silica gel column chromatography using hexane and chloroform (3:1) as the solvent. The target compound was obtained as a white solid (22.1 g, 85%). ^{1}H NMR, (200 MHz, $CDCl_3$) δ (ppm) 7.57−7.48, (m, 6H, aryl), 3.15 (t, J = 6.6 Hz, 4H), 2.19−2.11 (m, 4H), 1.21−1.06 (m, 4H); ^{13}C NMR (50 MHz, $CDCl_3$) δ (ppm) 150.8, 139.1, 131.1, 126.3, 122.1, 121.6, 54.6, 38.6, 33.8, 27.1; MS (EI-MS) m/z = 562 [M^+]. Anal. Calcd for $C_{19}H_{18}Br_4$: C, 40.32; H, 3.21. Found: C, 40.20; H, 3.12.

2,7-Bis(4,4,5,5-tetramethyl-[1,3,2]-dioxaborolane)-9,9-bis(3′-bromopropyl)fluorene (3). Under an argon atmosphere, 7-dibromo-9,9′-bis(3′′-bromopropyl)fluorene **2** (10 g, 17.7 mmol), bis(pinacolato)-diboron (13.5 g, 53 mmol), KOAc (15.6 g, 159 mmol), and [1,1′-bis(diphenylphosphino)ferrocene]dichloropalladium (1.5 g, 1.77 mmol) were dissolved in dioxane (250 mL). The reaction mixture was degassed by three "freeze−pump−thaw" cycles and then heated to 80 °C for 8 h. The dioxane was removed in vacuum followed by addition of CH_2Cl_2 and water. The aqueous phase was extracted with CH_2Cl_2 (2 × 400 mL), and then the combined CH_2Cl_2 solution was washed with water, brine water, and water, and then dried over $MgSO_4$. The solvent was removed under vacuum, and the residue was purified by column chromatography over silica gel using hexane/dichloromethane (3:1) to give **3** as a white solid (10 g, 86%). ^{1}H NMR, (200 MHz, $CDCl_3$) δ (ppm) 7.86−7.71 (m, 6H, aryl), 3.08 (t, J = 7.0 Hz, 4H), 2.23−2.15 (m, 4H), 1.40 (s, 24H), 1.17−1.03 (m, 4H); ^{13}C NMR (50 MHz, $CDCl_3$) δ (ppm) 148.7, 143.9, 134.6, 129.0, 120.0, 84.1, 54.2, 38.8, 34.3, 27.4, 25.1; MS (EI-MS) m/z = 660 [M^+]. Anal. Calcd for $C_{31}H_{42}B_2Br_2O_2$: C, 56.41; H, 6.41. Found: C, 56.29; H, 6.40.

1,4-Dibromo-2,5-di[2-[2-(2-hydroxylethoxy)-ethoxy]ethoxyl]benzene (5). Under an argon atmosphere, compound **4** (7.0 g, 26.1 mmol), 2-[2-(2-chloroethoxy)ethoxy]ethanol (22 g, 131 mmol), K_2CO_3 (21.6 g, 156.5 mmol), and KI (45 mg, 0.27 mmol) were dissolved in DMF (150 mL). The reaction mixture was heated to 80 °C for 24 h. The mixture was filtered, and then the DMF was removed in vacuum. The

(43) Rye, H. S.; Dabora, J. M.; Quesada, M. A.; Mathies, R. A.; Glazer, A. N. *Anal. Biochem.* **1993**, *208*, 144.
(44) Ihmels, H.; Otto, D. *Top. Curr. Chem.* **2005**, *258*, 161.

residue was purified by column chromatography over silica gel by using dichloromethane/methanol (20:1) to give the compound **5** as an oil (11.6 g, yield: 83.4%). ^{1}H NMR, (200 MHz, $CDCl_3$) δ (ppm) 7.16, (s, 2H, aryl), 4.14 (t, J = 4.4 Hz, 4H), 3.89 (t, J = 4.2 Hz, 4H), 3.81−3.60 (m, 16H), 2.40 (t, J = 5.4 Hz, 2H); ^{13}C NMR (400 MHz, CD_2Cl_2) δ (ppm) 150.2, 118.9, 111.1, 72.6, 70.9, 70.3, 70.0, 69.5, 61.5. MS (EI-MS) m/z = 532 (M^+). Anal. Calcd for $C_{18}H_{28}Br_2O_8$: C, 40.62; H, 5.30. Found: C, 40.64; H, 5.28.

1,4-Dibromo-2,5-di[2-[2-(2-tosylethoxy)ethoxy]ethoxyl]benzene (6). Under an argon atmosphere, compound **5** (5.5 g, 10.34 mmol), *N*,*N*-dimethylamino pyridine (DMAP) (250 mg, 2.0 mmol), and triethylamine (4.23 g, 41.8 mmol) were dissolved in 50 mL of dichloromethane, and the mixture was cooled down to 0 °C. Then *p*-toluenesulfonyl chloride (4,73 g, 24.8 mmol) was added in portions. The reaction mixture was stirred at room temperature overnight. The solvents were removed under vacuum, and the residue was purified by column chromatography over silica gel by using dichloromethane/methanol (20:1) to give compound **6** (8.16 g, 94%). ^{1}H NMR, (200 MHz, $CDCl_3$) δ (ppm) 7.83−7.77, (m, 4H, aryl), 7.37−7.31, (m, 4H, aryl), 7.14, (s, 2H, aryl), 4.19−4.08 (m, 8H), 3.85 (t, J = 4.4 Hz, 4H), 3.74−3.58 (m, 12H), 2.44 (s, 6H); ^{13}C NMR (100 MHz, CD_2Cl_2) δ (ppm) 150.2, 145.1, 132.9, 129.9, 127.8, 118.9, 111.1, 71.2, 70.7, 70.4, 70.1, 69.5, 68.6, 21.4. MS (ESI-MS): m/z = 861 ([M + Na]$^+$). Anal. Calcd for $C_{32}H_{40}Br_2O_{12}S_2$: C, 45.72; H, 4.80. Found: C, 45.67 H, 4.75

1,4-Dibromo-2,5-di[2-[2-(2-bromoethoxy)ethoxy]ethoxyl] benzene (7). Under an argon atmosphere, compound **6** (5.0 g, 5.95 mmol) and lithium bromide (4.13 g, 47.6 mmol) were dissolved in 50 mL of acetone. The mixture was then heated to reflux overnight. The solvent was removed, and water (50 mL) and dichloromethane (200 mL) were added. The organic layer was washed with water and dried over $MgSO_4$, and the solvent was removed under vacuum. The residue was purified by column chromatography over silica gel by using dichloromethane/methanol (30:1) to give compound **7** (2.5 g, 64.3%). ^{1}H NMR, (200 MHz, $CDCl_3$) δ (ppm) 7.16, (s, 2H, aryl), 4.14 (t, J = 4.4 Hz, 4H), 3.92−3.68 (m, 16H), 3.49 (t, J = 6.4 Hz, 4H); ^{13}C NMR (100 MHz, CD_2Cl_2) δ (ppm) 150.2, 118.9, 111.1, 71.1, 70.9, 70.5, 70.1, 69.5, 31.0. MS (EI-MS) m/z = 658 (M^+). Anal. Calcd for $C_{18}H_{26}Br_4O_6$: C, 32.86; H, 3.98. Found: C, 32.97; H, 4.04.

General Procedure for the Preparation of poly1$_{20}$N and poly1$_{10}$N. The neutral polymers were prepared by a palladium-catalyzed Suzuki cross-coupling reaction. The purified monomers **3**, **7**, and **8** (4,7-dibromo-2,1,3-benzothiadiazole) were mixed in the appropriate ratios with $Pd(PPh_3)_4$ (1 mol %) in a mixture of 2 M K_2CO_3 (aq) (5 equiv/Br) and toluene (1/2 v/v) under argon. The monomer concentration in toluene is around 0.07 M. The reaction mixture was degassed by three "freeze−pump−thaw" cycles and then heated to 95 °C for 24 h. After cooling to room temperature, acetone was added into the mixture. The precipitate was separated by filtration and washed with methanol and acetone. Purification was accomplished by precipitation of chloroform solutions into methanol. The neutral polymers were obtained by filtration and drying under vacuum for 24 h as bright-yellow powders.

Poly1$_{20}$N (yield, 72%). ^{1}H NMR (200 MHz, $CDCl_3$) δ (ppm) 8.09−7.73 (m, 34H), 7.18 (s, 6H), 4.21 (m, 12H), 3.84−3.69 (m, 48H), 3.46 (t, J = 6.0 Hz, 12H), 3.24 (m, 20H), 2.31 (m, 20H), 1.38 (m, 20H); ^{13}C NMR (100 MHz, $CDCl_3$) δ (ppm) 154.4, 150.6, 150.1, 149.8, 149.3, 149.1, 141.3, 140.0, 137.6, 133.6, 131.4, 129.2, 128.3, 124.3, 119.9, 117.2, 71.5, 70.8, 70.1, 69.4, 54.4, 39.0, 34.9, 30.7, 27.7; GPC (THF, relative to polystyrene standards), M_w = 77 708 g/mol; M_n = 26 340 g/mol; polydispersity index, 2.9. Elemental analysis calculated: C, 50.94; H, 4.62; N, 1.48. Found: C, 51.76; H, 4.59; N, 1.40.

Poly1$_{10}$N (yield, 84%). ^{1}H NMR (200 MHz, $CDCl_3$) δ (ppm) 8.06−7.72 (m, 32H), 7.18 (s, 8H), 4.20 (m, 16H), 3.84−3.69 (m, 64H), 3.46 (t, J = 6.0 Hz, 16H), 3.22 (m, 20H), 2.27 (m, 20H), 1.34 (m, 20H); ^{13}C NMR (50 MHz, CDCl3) δ (ppm) 150.6, 149.1, 140.0, 137.6, 131.4, 129.2, 124.3, 119.9, 117.2, 71.5, 70.8, 70.1, 69.4, 54.3, 38.8, 34.8, 30.7, 27.7; GPC (THF, relative to polystyrene standards), M_w = 126 102 g/mol; M_n = 47 608 g/mol; polydispersity index, 2.6. Elemental analysis calculated: C, 49.95; H, 4.80; N, 0.67. Found: C, 50.15; H, 4.87; N, 0.60.

General Synthesis Procedure for Compounds poly1$_{20}$ and poly1$_{10}$: Condensed trimethylamine (8 mL) was added dropwise to a solution of the neutral precursor polymer (100 mg) in 20 mL of THF at −78 °C. The mixture was then allowed to warm up to room temperature for 4 h. The precipitate was redissolved by addition of methanol (20 mL). After the mixture was cooled down to −78 °C, more trimethylamine (6 mL) was added and the mixture was stirred for 24 h at room temperature. After most of the solvent was removed, acetone was added to precipitate the polymers as a light orange powder.

Poly1$_{20}$ (yield, 85%). ^{1}H NMR (200 MHz, d^6-DMSO) δ (ppm) 8.34−7.82 (m, 34H), 7.27 (br, 6H), 4.32 (br, 12H), 3.90−3.03 (m, 224H), 2.31−1.91 (m, 20H), 1.75−1.30 (m, 20H). Elemental analysis calculated: C, 53.02; H, 6.82, N, 5.89. Found: C, 52.89; H, 6.78; N, 5.80

Poly1$_{10}$ (yield, 87%). ^{1}H NMR (200 MHz, d^6-DMSO) δ (ppm): 8.37−7.25 (m, 40H), 4.30 (br, 16H), 3.89−3.06 (m, 262H), 2.18(m, 20H), 1.35 (m, 20H). Elemental analysis calculated: C, 52.19; H, 6.95; N, 5.36. Found: C, 52.07; H, 6.87; N, 5.43.

Acknowledgment. The authors would like to thank Drs. Dmitry Korystov, Janice Hong, Brent Gaylord, Renqiang Yang, and Fuke Wang for helpful and important discussions. The work received financial support from the NSF (DMR 0606414) and from the Institute for Collaborative Technologies.

Supporting Information Available: Dependence of the PL spectra of **poly1$_{20}$** vs [RU], PL spectra of **poly1$_0$** upon addition of [dsDNA], PL spectra of **poly1$_{20}$** upon addition of [dsDNA] to generate Figure 8, PL spectra of **poly1$_{20}$** upon addition of [dsDNA] in buffer, comparison of δ vs [dsDNA] for **poly1$_{10}$** and **poly1$_{20}$**, and plots of δ vs [dsDNA] for **poly1$_{10}$** as a function of $[RU]_0$. This material is available free of charge via the Internet at http://pubs.acs.org.

JA072471S